Electronic Supplementary Material (ESI) for Journal of Materials Chemistry A.

Supporting Information

Stress induced to shrink ZIF-8 derived hollow Fe-NC supports synergizes with Pt nanoparticles to promote oxygen reduction electrocatalysis

Wei Liao, Shangyan Zhou, Zhengcheng Wang, Jin Long, Meida Chen, Qian Zhou, Qingmei Wang*

Guizhou University Key Laboratory of Green Chemical and Clean Energy Technology, School of Chemistry and Chemical Engineering, Guizhou University, Guiyang, Guizhou, 550025, China.

*Corresponding Author: wqm0702@outlook.com

Characterization

The as-prepared catalyst was characterized by X-ray diffraction (XRD) by D8 DISCOVER (Bruker AXS, Germany). The transmission electron microscopy (TEM) and high-resolutions TEM (HRTEM) were implemented to confirm the microstructure by JEMARM200 F microscope manipulating at 200 kV. The high angle annular dark-field scanning transmission electron (HAADF-STEM) images were recorded with JEMARM200 F manipulating at 300 kV. The energy-dispersive X-ray spectroscopy (EDX) elemental mapping was conducted to characterize the element distribution of different elements. The spectrometer was installed in JEMARM200 F transmission electron microscope (HAADF-STEM) and manipulated at 200 kV. Inductively coupled plasma mass spectrometry (ICP-MS) was manipulated to assess the concentration of the catalyst on PerkinElmer Optima 5300DV apparatus. The X-ray photoelectron spectrum (XPS) testing was implemented by K-Alpha Plus (Somerfield, USA) with Al-Ka X-ray as the illuminant.

Electrochemical tests. Electrochemical analysis was operated in a standard three-electrode system by applying an electrochemical work station (Donghua test, Dh7003). The standard three-electrode is formed of the working electrode (glassy carbon (GC)), reference electrode (Ag/AgCl) and counter electrode (carbon rod). All potentials, unless mentioned otherwise, were transformed to the reversible hydrogen electrode (RHE). To obtain the catalyst ink, 2 mg of the catalyst was dissolved in the mixed solutions, which contained ethanol (0.8 mL) and Nafion solutions (0.005 mL), and then ultrasonicated for 0.5h. 15 mL uniform solutions obtained after ultrasonic treatment was applied to the GC which was polished with alumina and dried in room temperature, obtaining ~2.5 ug Pt loading. The cyclic voltammetry (CV) was carried out by employing cyclic scans between 0.05 to 1.2 V (vs RHE) in fresh by N_2 0.1 M $HClO_4$ electrolyte solutions (sweep rate: 0.05V/s). The oxygen reduction reaction (ORR) analysis was implemented in saturated-O_2 0.1 M $HClO_4$ electrolyte solutions (sweep rate: 0.05V/s; rotating speeds: 1600 rpm). The CO stripping experiments were operated in 0.1 M $HClO_4$ electrolyte

solutions. The CO gas was bubbled into electrolyte solutions about 20 min. Then the dissolved CO was purified using N_2 for 0.5h in the 0.1 M $HClO_4$ electrolyte solutions. The accelerated durability test (ADT) was executed in saturated-O_2 0.1 M $HClO_4$ solutions, and a cyclic potential scan of 20,000 CV cycles was performed between 0.6 and 1.2 V.

According to the peak area of CO stripping and the loading quantity of Pt on the electrode, we calculated the electrochemical surface area (ECSA) of the catalysts via the following equation:

$$ECSA_{CO} = \frac{Qco}{0.42*[Pt]}$$

Q_{CO} (mC/cm^2) refers to the electric quantity calculated by the integral of CO stripping peak. The [Pt] refers to the loading quantity of Pt on the electrode (mg/cm^2). The constant 0.42 (mC/cm^2) indicates the CO charge per unit area (cm^2) of Pt surface.

Computational details

All spin-polarization periodic density functional theory (DFT) calculations were performed within the frame of Vienna ab initio simulation package (VASP).[1] The projector augmented wave (PAW) method. The projector augmented wave (PAW) method[2] was used to describe the ionic cores. And the generalized gradient approximation (GGA) with the Perdew-Burke-Ernzerhof (PBE) exchange-correlation functional[3] were employed to model the electron exchange-correlation. A cutoff energy of 450 eV was used for the plane-wave basis set. The convergence criterion was 10−5 eV for energy and 0.02 eV/Å for force. 2×3×1 Monkhorst-Pack grid k-points was employed for all DFT calculation. For all slab models, Wan der Waals effects were applied using Grimme's DFT-D3 correction method, and dipole corrections along the surface were considered.

The Carbon substrate was simulated by using a periodic graphene slab model which contains 80 C atoms and with 18 Å vacuum layer along the z-direction. Based on the assumption that FeN_4 is the dominant species in Fe-N-C catalysts produced by pyrolysis of Fe-doped ZIF-8@PDA composites, the FeN_4 was introduced into the above graphene slab to represent Fe-N-C material. Besides, a Pt6 cluster was constructed to

serve as Pt particle interacted with C contained materials.

The ORR process contains following steps:

$$* + O_2 + H_2O \rightarrow *OOH + OH^- - e^- \quad (1)$$

$$*OOH \rightarrow *O + OH^- - e^- \quad (2)$$

$$*O + H2O \rightarrow *OH + OH^- - e^- \quad (3)$$

$$*OH \rightarrow * + OH^- - e^- \quad (4)$$

The adsorption free energy of ORR intermediates were calculated using the equations:

$$\Delta G_{*OOH} = G_{*OOH} + \frac{3}{2} G_{H_2} - G_* - 2G_{*H_2O}$$

$$\Delta G_{*O} = G_{*O} + G_{H_2} - G_* - G_{*H_2O}$$

$$\Delta \mathrm{G_{*OH}} = \mathrm{G_{*OH}} + \frac{1}{2} \mathrm{G_{H_2}} - \mathrm{G_*} - \mathrm{G_{*H_2O}}$$

The Gibbs free energy G of each species was calculated as follow:

$$\mathrm{G = E + ZPE - TS}$$

where G, E, ZPE and TS are the free energy, total energy from DFT calculations, zero point energy and entropic contributions (T was set to be 300K), respectively. ZPE and TS could be derived after frequency calculation.

Further, the free energy change of each steps were calculated using:

$$\Delta G_1 = 4.92 - \Delta G_{*OOH} - eU$$

$$\Delta G_2 = \Delta G_{*OOH} - \Delta G_{*O} - eU$$

$$\Delta G_3 = \Delta G_{*O} - \Delta G_{*OH} - eU$$

$$\Delta G_4 = \Delta G_{*OH} - eU$$

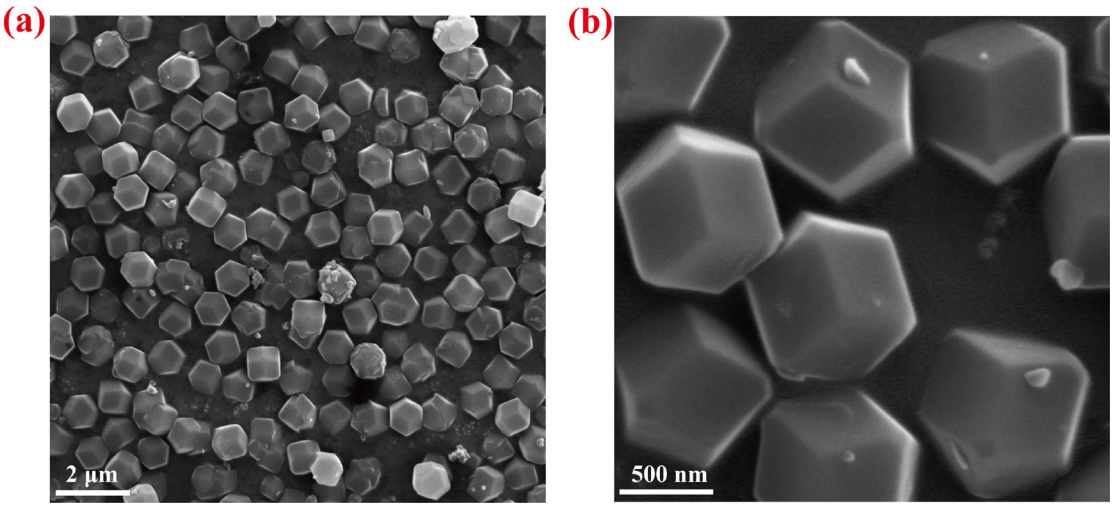

Figure S1. TEM image of the synthesized ZIF-8 precursor.

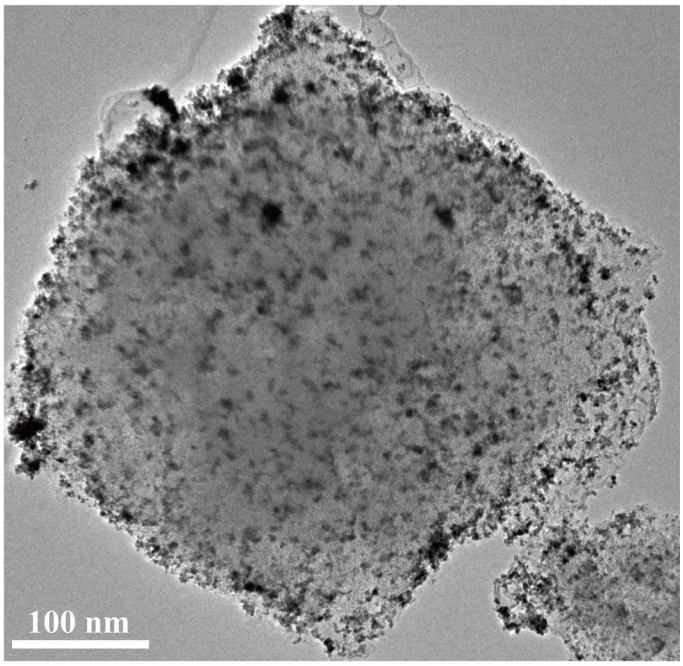

Figure S2. TEM images of Pt@Fe-NC(ZIF) sample.

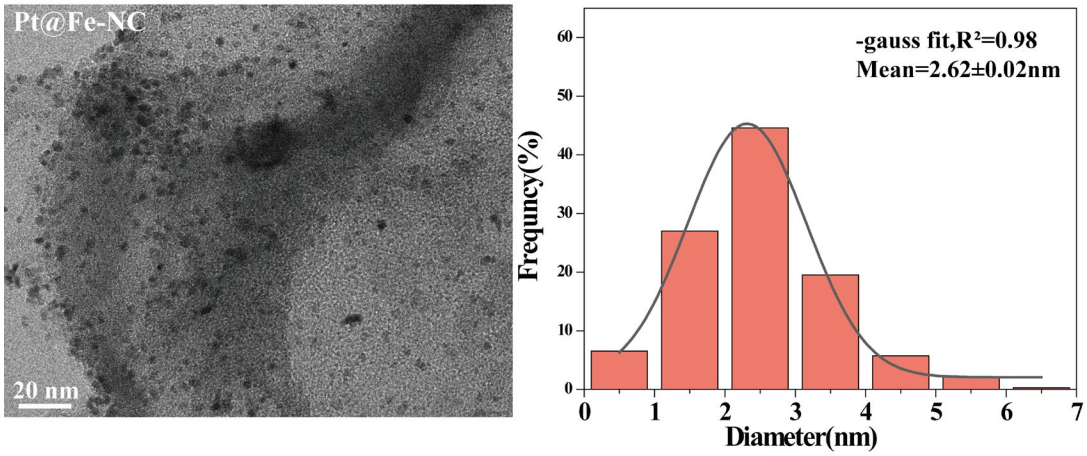

Figure S3. TEM image of the catalyst and the corresponding particle size statistical histogram.

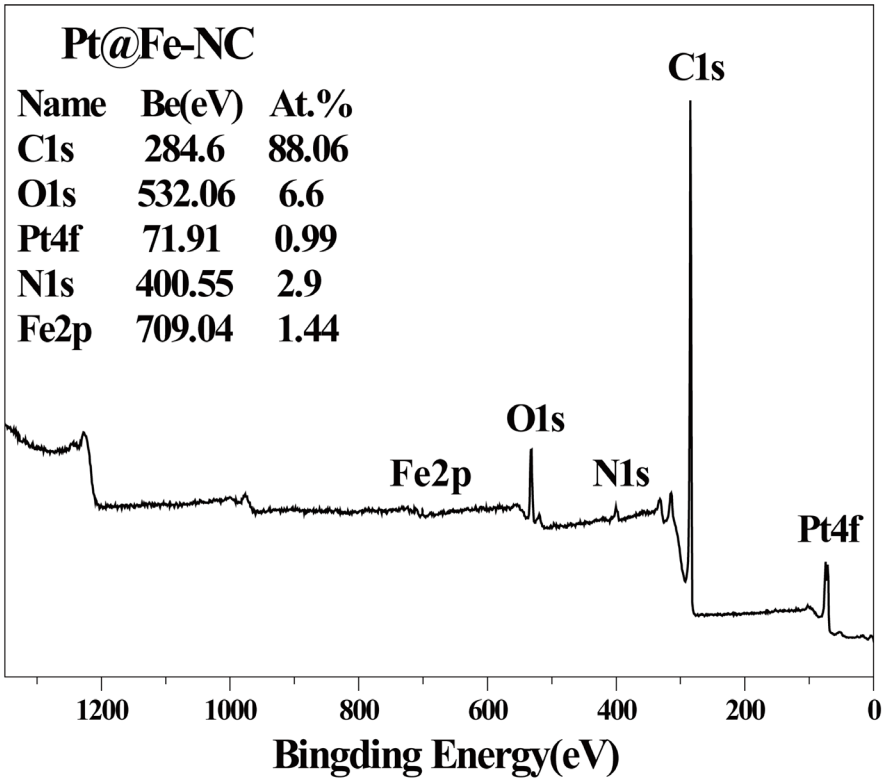

Figure S4. XPS spectrum of Pt@Fe-NC catalyst.

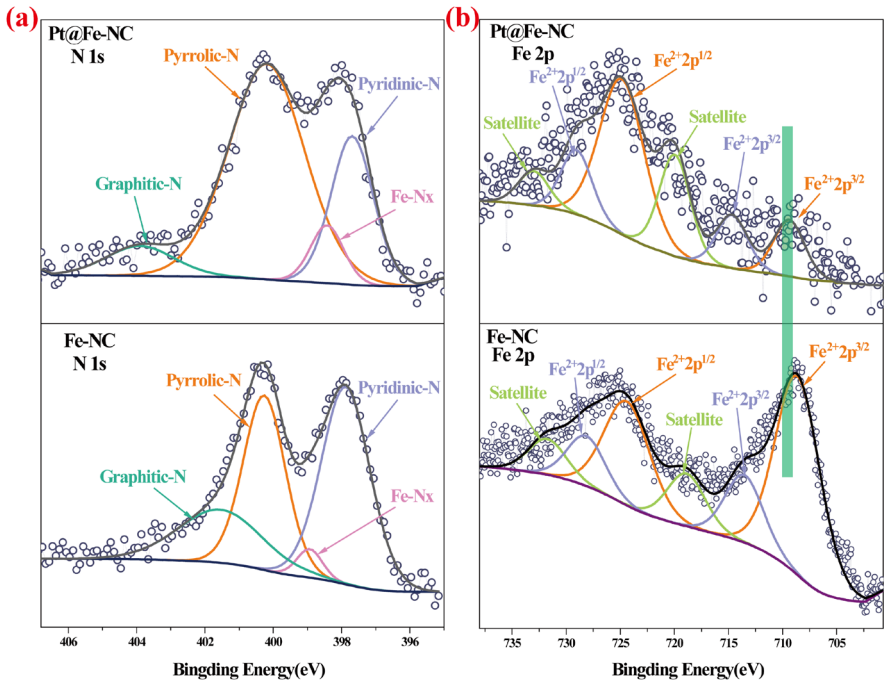

Figure S5. High-resolution XPS spectra of N 1s (a) and Fe 2p (b) of Pt@Fe-NC and Fe-NC.

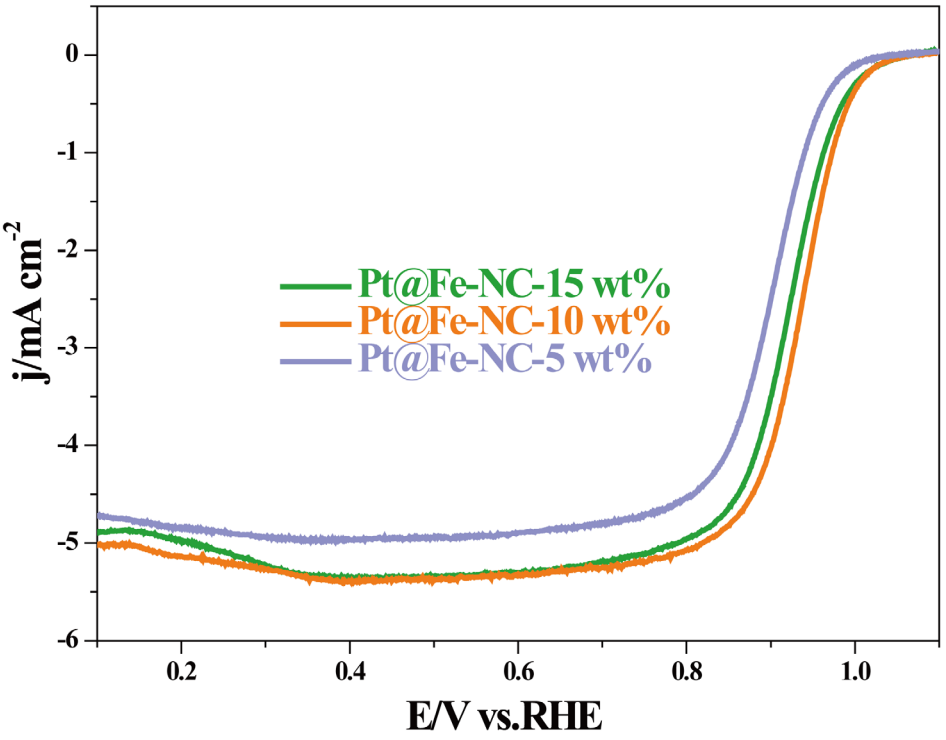

Figure S6. ORR curves of Pt@Fe-NC-15 wt%, Pt@Fe-NC-10 wt% and Pt@Fe-NC-5 wt% samples.

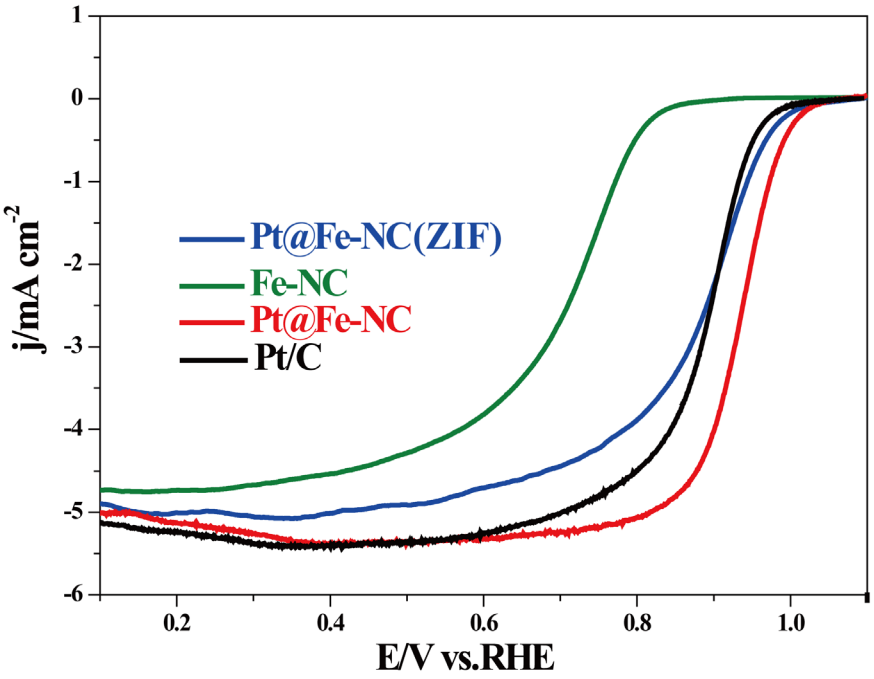

Figure S7. ORR polarization curves of Pt@Fe-NC, Pt@Fe-NC$_{ZIF}$, and Fe-NC samples.

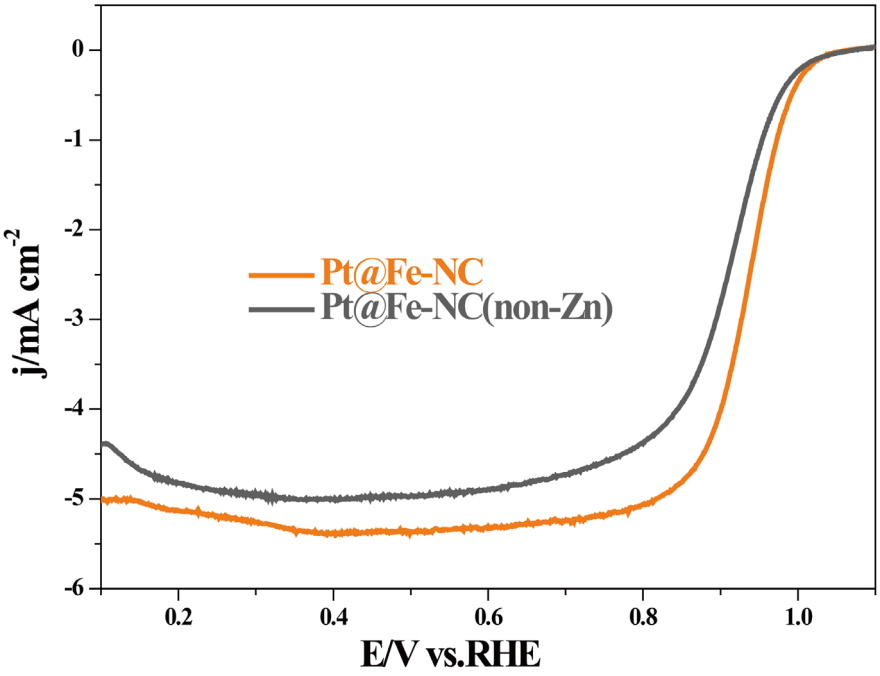

Figure S8. ORR curves of Pt@Fe-NC and Pt@Fe-NC(non-Zn) samples.

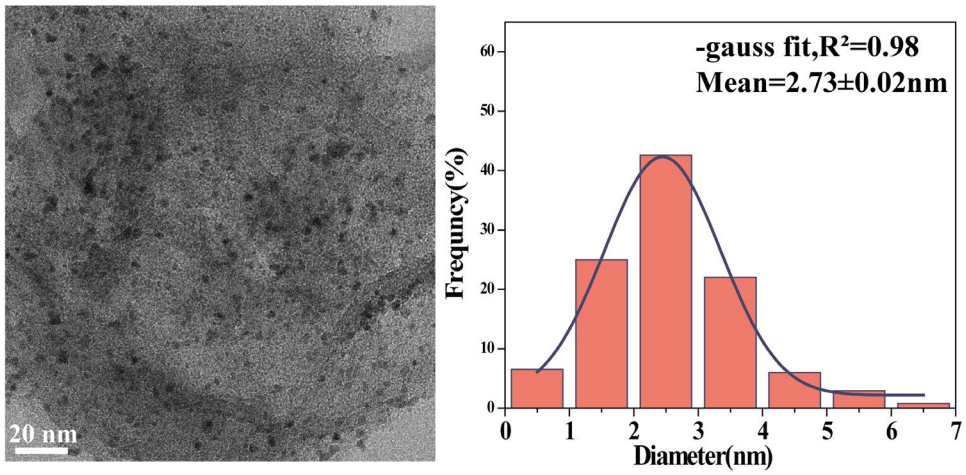

Figure S9. TEM image of Pt@Fe-NC catalyst after ADT test and corresponding particle size statistical histogram.

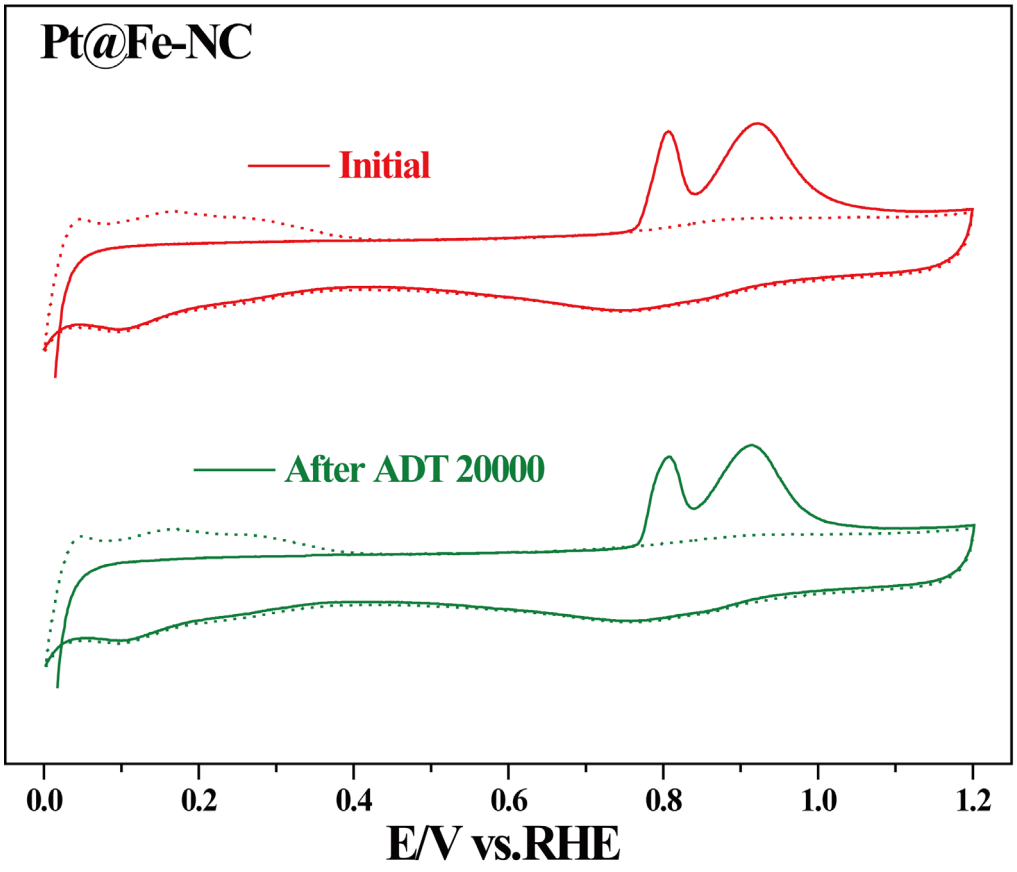

Figure S10. CO-striping plots of Pt@Fe-NC catalyst after ADT test.

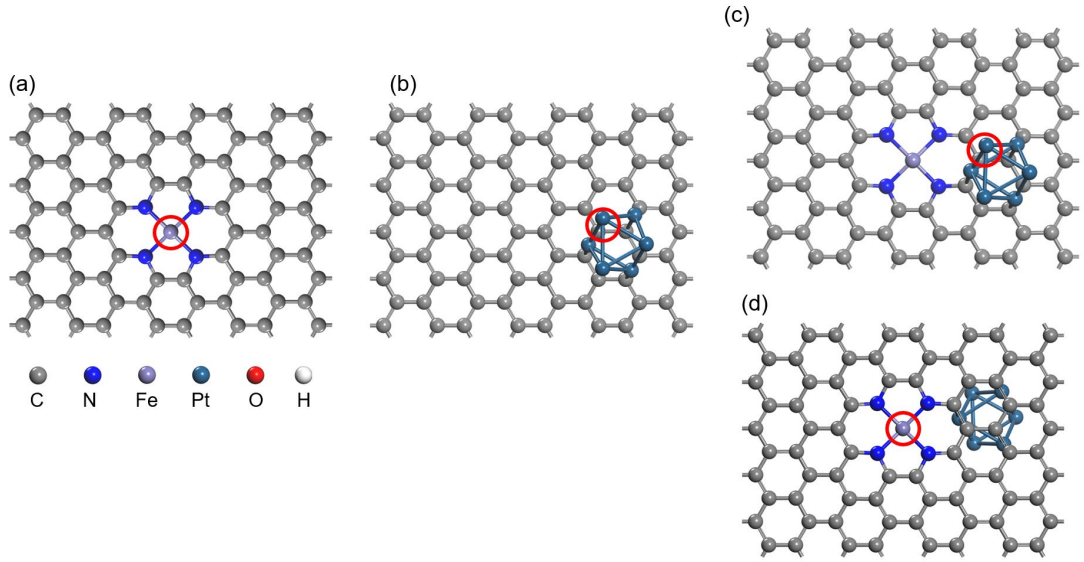

Figure S11. Top-view of (a) FeN_4, (b) Pt/C, (c) Pt@FeN_4-C (Pt site) and (d) Pt@FeN_4-C (Fe site). Red circle represents the adsorption site of initial ORR intermediate (i.e. OOH)

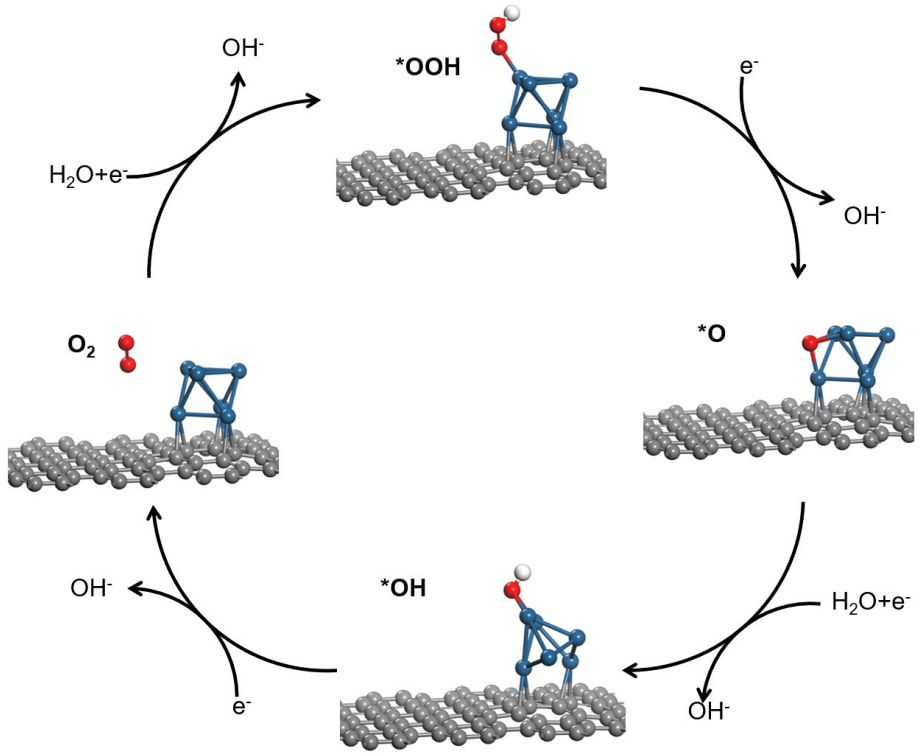

Figure S12. The reaction scheme of ORR process on Pt site of Pt/C.

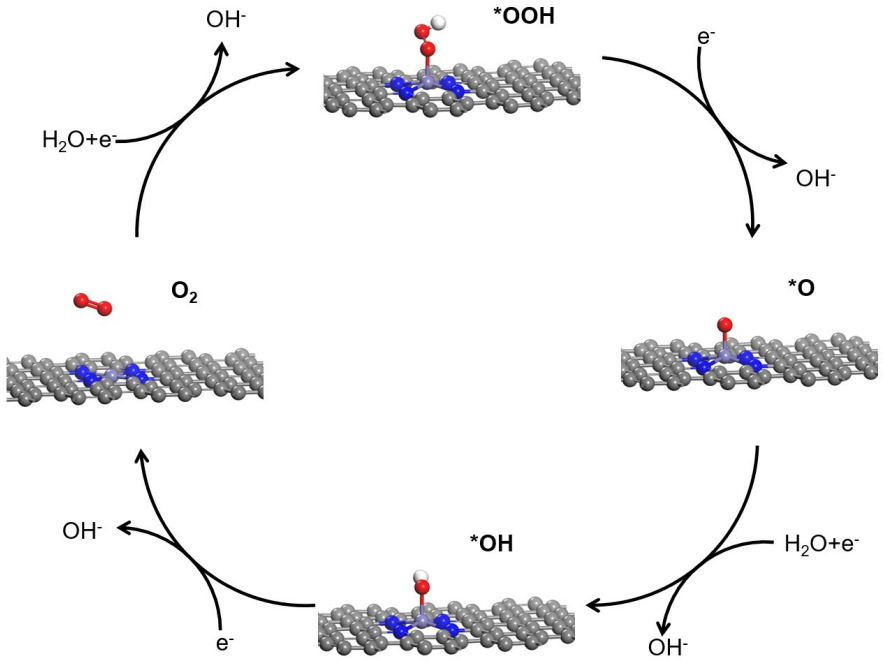

Figure S13. The reaction scheme of ORR process on Fe site of FeN_4-C.

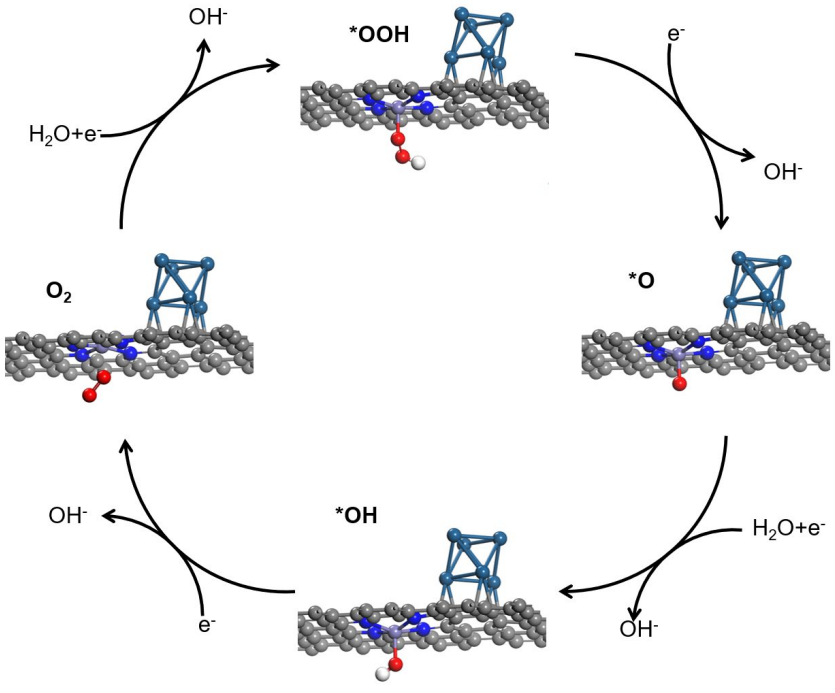

Figure S14. The reaction scheme of ORR process on Fe site of Pt@FeN_4-C.

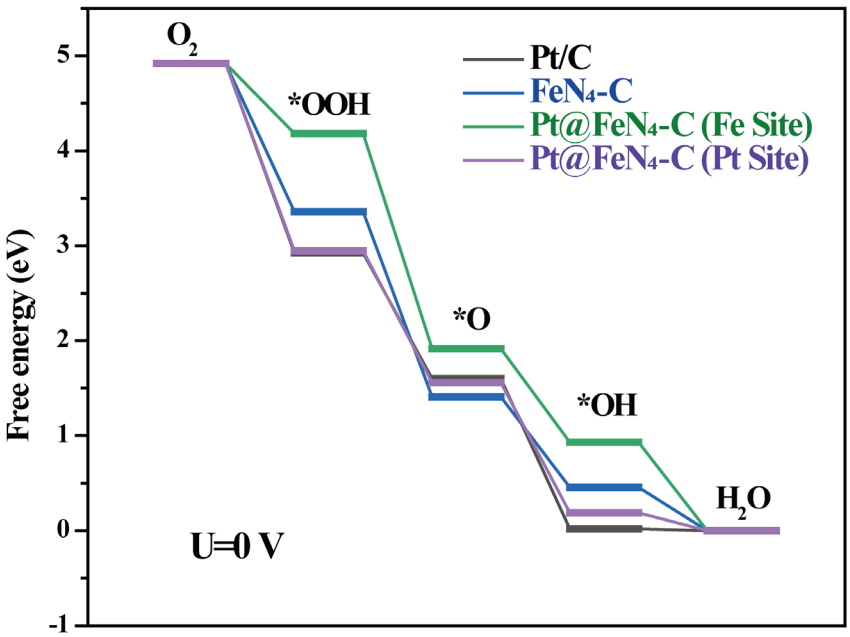

Figure S15. Free-energy diagram of the ORR pathways at U=0 V.

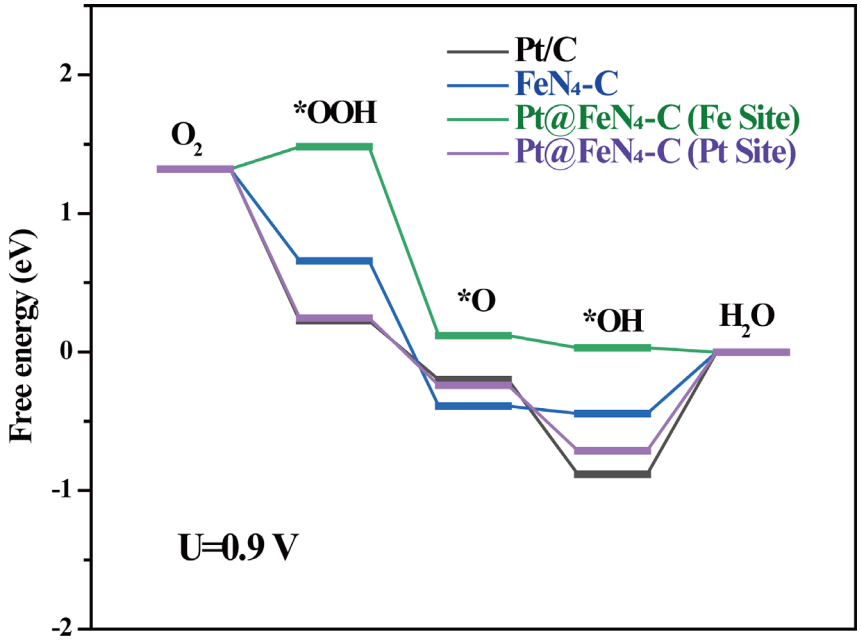

Figure S16. Free-energy diagram of the ORR pathways at U=0.9 V.

Table S1. Pt loading of catalyst and CO Stripping Onset Potential(V), $ECSA_{CO}$, half-wave potential, mass activity and specific activity at 0.9V of commercial Pt/C, Pt@HNC-B and Pt@HNC-A catalysts.

Sample	Pt loading of catalyst (ICP)	CO Stripping Onset Potential(V)	$ECSA_{CO}$ (m^2/g)	Halfwave potential(V)	Mass activity@0.9V(A/mg_{Pt})	Specific activity@0.9V(mA/cm^2)
Pt/C	20 wt%	0.781	69.12	0.893	0.198	0.286
Pt@Fe-NC	10 wt%	0.749	77.79	0.936	1.34	1.72

Table S2. Comparison of the ORR performance of the as-prepared catalysts with recently published papers.

Catalysts	Half-wave (V vs RHE)	MA (A/mg_{pt})	SA (mA/cm^2)	Electrolytes	References
Pt_A@Fe_{SA}-N-C	0.923	≈0.85	≈1.35	0.1 M $HClO_4$	4
Pt/FeN_4-C	0.9	≈0.6	≈1.5	0.1 M $HClO_4$	5
PtCo-PtSn/C	0.930	1.158	----	0.1 M $HClO_4$	6
Ni_3N@Pt_{shell}/C	0.88	1.12	1.18	0.1 M $HClO_4$	7
Pd-Pt great icosahedra	≈0.92	1.23	0.99	0.1 M $HClO_4$	8
Core-shell d-PtCo/NDCS	0.933	0.956	0.83	0.1 M $HClO_4$	9
Pt@Fe-N/R3DG	0.87	----	2.22	0.1 M KOH	10
$Pt_{78}Zn_{22}$/KB	≈0.92	1.18	3.65	0.1 M $HClO_4$	11
Pt@Fe-NC	**0.936**	**1.34**	**1.72**	**0.1 M $HClO_4$**	**This work**

Table S3. Comparison of commercial Pt/C and Pt@HNC-B and Pt@HNC-A catalysts ORR activity before and after aging for 5000, 10000, 20000 CV cycles.

Sample		Halfwave potential(V)	$ECSA_{CO}$ (m^2/g)	Mass activity@0.9v(A/mg_{Pt})	Specific activity@0.9 V(mA/cm^2)
Pt/C	Initial	0.893	69.12	0.198	0.286
	After 20K CV cycles	0.845	40.02	0.078	0.195
Pt@Fe-NC	Initial	0.936	77.79	1.34	1.72
	After 20K CV cycles	0.924	69.24	1.15	1.66

References

1 G. Kresse and J. Furthmüller, *Phys. Rev. B*, 1996, **54**, 11169-11186.

2 P. E. Blöchl, *Phys. Rev. B*, 1994, **50**, 17953-17979.

3 J. P. Perdew, K. Burke and M. Ernzerhof, *Phys. Rev. Lett.*, 1996, **77**, 3865-38684

4 X. Ao, W. Zhang, B. Zhao, Y. Ding, G. Nam, L. Soule, A. Abdelhafiz, C. Wang and M. Liu, *Energy Environ. Sci.*, 2020, **13**, 3032-3040.

5 Z. Qiao, C. Wang, C. Li, Y. Zeng, S. Hwang, B. Li, S. Karakalos, J. Park, A. J. Kropf, E. C. Wegener, Q. Gong, H. Xu, G. Wang, D. J. Myers, J. Xie, J. S. Spendelow and G. Wu, *Energy Environ. Sci*, 2021, **14**, 4948-4960.

6 J. Chen, G. Qian, B. Chu, Z. Jiang, K. Tan, L. Luo, B. Li and S. Yin, *Small*, 2022, **18**, 2106773.

7 H.-Y. Jeong, D.-g. Kim, S. G. Akpe, V. K. Paidi, H. S. Park, S.-H. Lee, K.-S. Lee, H. C. Ham, P. Kim and S. J. Yoo, *ACS Appl. Mater. Interfaces*, 2021, **13**, 24624-24633.

8 M. Liu, Z. Lyu, Y. Zhang, R. Chen, M. Xie and Y. Xia, *Nano Lett.*, 2021, **21**, 2248-2254.

9 Z. Chen, C. Hao, B. Yan, Q. Chen, H. Feng, X. Mao, J. Cen, Z. Q. Tian, P. Tsiakaras and P. K. Shen, *Adv. Energy Mater.*, 2022, 2201600.

10 Y. Qin, L. Chao, J. J. He, Y. Liu, F. Chu, J. Cao, Y. Kong and Y. Tao, *J. Power Sources*, 2016, **335**, 31-37.

11 M. Liu, B.-A. Lu, G. Yang, P. Yuan, H. Xia, Y. Wang, K. Guo, S. Zhao, J. Liu, Y. Yu, W. Yan, C.-L. Dong, J.-N. Zhang and S. Mu, *Adv. Sci.*, 2022, **9**, 2200147.